



International Journal of Innovative Research in Science Engineering and Technology (IJIRSET)

(A Monthly, Peer Reviewed, Refereed, Scholarly Indexed, Open Access Journal)



Impact Factor: 8.699

Volume 14, Issue 3, March 2025

CFD Analysis of NACA2412 Airfoil

S.V.Sheno Shallen^{*a}, P. Logesh^a, V.Ranjith^a, R.Ranjith^a, V. Sanjay^a, P. Velmurugan^b, S. Saravanan^b

B.E Student, Department of Mechanical Engineering, Annamalai University, Annamaaianagar, Tamil Nadu, India^a

Faculty, Department of Mechanical Engineering, Annamalai University, Annamaaianagar, Tamil Nadu, India^b

ABSTRACT: In this study, the effect of different angle of attack (0 and 6 degrees) on the NACA 2412 airfoil was investigated numerically using Ansys Fluent 2024. The lift coefficient, lift to drag ratio and pressure distribution obtained by numerical simulation is correlated with the published experimental results. The simulation was performed at a Reynolds number, Re , of 3×10^6 . The analysis of the two-dimensional subsonic flow over a NACA 2412 airfoil at various angles of attack and operating at a Reynolds number of 3×10^6 is presented. The simulation results show close agreement with the experimental outcome, confirming numerical simulation is a reliable alternative to experimental method in determining lift and drag in NACA 2412 airfoil.

KEYWORDS: Aerodynamics; Airfoil; CFD; NACA.

I. INTRODUCTION

Airfoils plays an important role in aerodynamic applications as the performance of a body is influenced its aerodynamic shape . Airfoils are extensively employed in different areas, such as wind turbine blades, axial compressor and fan blades, propellers, and wings . While designing a complete aerodynamic body, it is essential to design or employ the designated airfoil depending on the application. Airfoils are critical in aerodynamic design, influencing lift, drag, and stability in aircraft, wind turbines, and other systems [1]. Few of the salient research attempted in airfoil design to improve efficiency are presented here. In 2014, Cakmakcioglu et al.[2] numerically studied the flow taking place over the NREL S826 airfoil at low Reynolds numbers and found computational Fluid Dynamics (CFD) results are in fair agreement with experimental results. In a similar attempt, Patel et al.[3] analyzed the flow around the NACA 0012 airfoil and reported similar results. In another attempt, Sreejith and Sathyabhama [4] while studying the effect of boundary layer trips on the aerodynamic behavior of E216 airfoil, concluded that the boundary layer suppresses the laminar bubbles and thereby improve the aerodynamic performance. Li et al.[5] designed a wind turbines airfoil for lower wind speed and concluded that the designing airfoils for site-specific blade requirements are possible. Matyushenko et al.[5]studied the flow pattern around various airfoils having different shapes and thicknesses using two-dimensional RANS, found good agreement between computational results and the experiment for angles of attack between 7-12°.

The NACA airfoil series, developed by the National Advisory Committee for Aeronautics, offers standardized shapes defined by a four-digit number. This number encodes the maximum camber, the position of maximum camber, and the maximum thickness. The NACA 2124 is a thicker airfoil with moderate camber, potentially suitable for low-speed flight regimes or applications requiring enhanced structural integrity, such as certain light aircraft or wind turbine blades [6].NACA 2124 is 24% thicker than many standard airfoils, which typically range from 10% to 15% thickness . Thicker airfoils can offer structural advantages, reducing the need for internal reinforcements and potentially lowering manufacturing costs [7]. They are often considered for low-speed aircraft, where high lift at low speeds is crucial, or for applications where drag is less critical compared to structural needs [8]. The 2% camber at 10% chord suggests it has some lift-enhancing curvature, which could be beneficial at low angles of attack. Based on the literature, it is inferred that more studies are devoted to airfoils different airfoil while studies on NACA 2124 airfoil is limited. Hence, the CFD study on determining the NACA 2124 airfoil characteristics is essential and hence attempted.

II. MATERIAL AND METHOD

A body moving through air is constantly subjected to aerodynamic forces, specifically lift, drag, thrust, and weight [10]. These forces are significantly affected by the body's shape and the motion of the surrounding air [11]. An airfoil, which is the cross-sectional profile of a wing or blade, is utilized across multiple applications. Typically, airfoils are engineered to generate lower pressure above the wing, thereby producing lift. The lift is often expressed as a

dimensionless value known as the lift coefficient, calculable for airfoils via Equation 1. In this equation, F_L represents the lift force (N), ρ denotes air density (kg/m^3), V indicates wind speed (m/s), A is the swept area (m^2), and c stands for chord length (m). Likewise, the drag coefficient is determined using Equation 2, where F_D symbolizes the drag force (N). The pressure coefficient is derived from Equation 3, with ΔP representing the pressure differential (Pa) [12].

$$C_L = \frac{F_L}{0.5\rho V^2 c} \quad (1)$$

$$C_D = \frac{F_D}{0.5\rho V^2 c} \quad (2)$$

$$C_P = \frac{\Delta P}{0.5\rho V^2} \quad (3)$$

1. Computational Fluid Dynamics Method:

Computational Fluid Dynamics is extensively applied in various fields where fluid flow is a primary concern. In this study, the CFD approach is employed to model the airflow surrounding airfoils. The fundamental equations in CFD encompass the conservation of mass, momentum, and energy. The Navier-Stokes equation, a vector-based expression, emerges from applying Newton's Law of Motion to a fluid element and is commonly referred to as the momentum equation [13]. This is complemented by the continuity equation, which ensures mass conservation (ANSYS 2024). The equations representing the conservation of mass and momentum are outlined in Equation 2 and Equation 3, respectively [14]. In Equation 4, the velocity vector \vec{V} , dependent on time (t) and spatial coordinates (x, y, z), includes local velocity components (u, v, w), while S_M denotes the source term. In Equation 5, p represents static pressure, $\vec{\tau}$ symbolizes the stress tensor, and $\rho \vec{g}$ and \vec{F} indicate the gravitational and external body forces, respectively. The formulation for the stress tensor $\vec{\tau}$ is provided in Equation 6, where μ signifies viscosity and I represent the identity tensor [15].

$$\frac{\partial \rho}{\partial t} + \nabla \cdot (\rho \vec{V}) = S_M \quad (4)$$

$$\frac{\partial \rho}{\partial t} (\rho \vec{V}) + \nabla \cdot (\rho \vec{V} \vec{V}) = -\nabla p + \nabla \cdot (\vec{\tau}) + \rho \vec{g} + \vec{F} \quad (5)$$

$$\vec{\tau} = \mu \left[(\nabla \vec{V} + \nabla \vec{V}^T) - \frac{2}{3} \nabla \vec{V} \right] \quad (6)$$

2. Boundary Conditions and Mesh Generation:

The computational domain is composed of a semicircular region with a 30-meter radius and a rectangular section extending 60 meters in length. The airfoil is positioned at the center of the semicircle. The boundary conditions were established with a velocity inlet and a pressure outlet assigned to the inlet and outlet boundaries, respectively, while the airfoil surface was designated as a no-slip wall. Inlet velocities were determined based on the Reynolds number. The pressure was set to 1 atm, and the temperature was fixed at 15 °C. Under these conditions, the air density (ρ) is 1.225 kg/m^3 [16], and the dynamic viscosity (μ) is $1.802 \times 10^{-5} \text{ kg/(m}\cdot\text{s)}$ [16].

The computational domain was segmented into six distinct sections to establish a structured grid. Edge sizing was employed to generate a highly refined mesh surrounding the airfoil, the primary area of focus. For precise resolution of the airflow around the airfoil, the wall y^+ value was maintained below 1, a requirement dictated by the chosen turbulence model. Ultimately, a mesh comprising approximately 400,000 elements was generated, as shown in Figure 1.

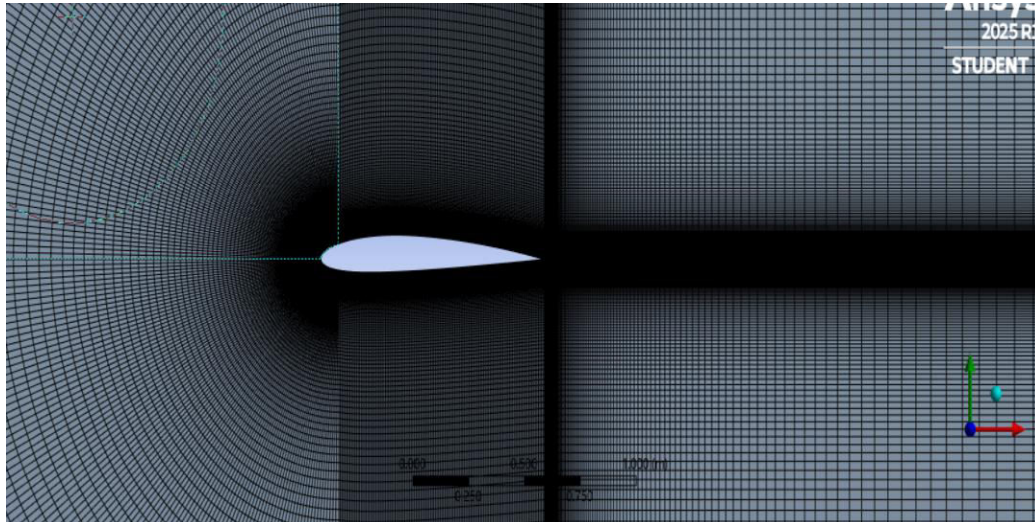


Fig.1 Mesh generation in airfoil

III. RESULTS

1.Static pressure over NACA 2412 Airfoil:

For a zero-degree angle of attack the contours of static pressure over an airfoil is asymmetrical at the top and bottom sections of the airfoil and the stagnation point prevails on the nose of the airfoil (Fig.3). Subsequently, a pressure difference is created between two faces of airfoil and some amount of lift is being generated. This phenomenon is consistent with previous studies. On top of the airfoil the pressure is -6.94×10^{-2} Pa and at the bottom of the aircraft the pressure is -1.34×10^{-2} .

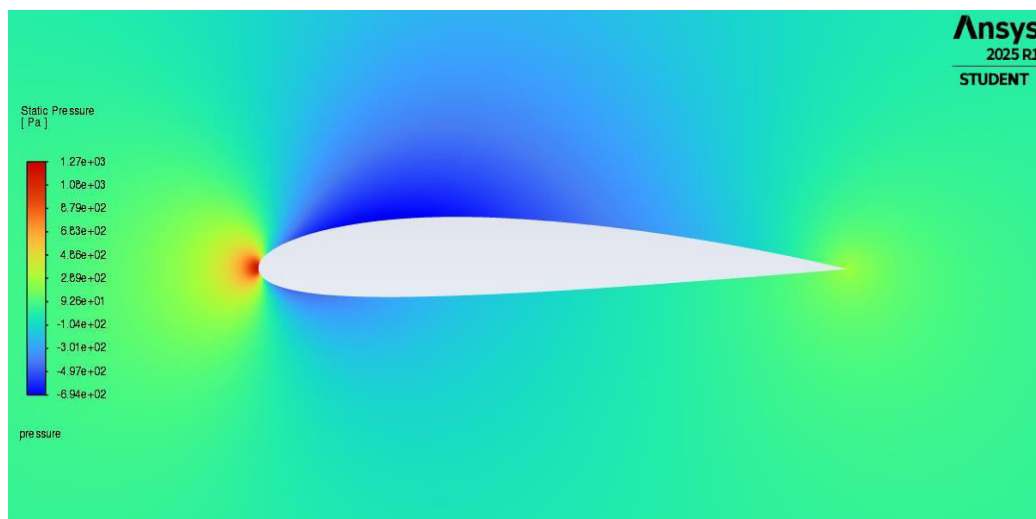


Fig.2: Static pressure contour over NACA 2412 airfoil at 0 degree of AOA

For an angle of attack of 6 degrees, the flow has a stagnation point just under the leading edge and hence producing lift as there is a low-pressure region on the upper surface of the foil as shown in Figure 2. it can also be observed that Bernoulli's principle is holding true; the velocity is high (denoted by the red contours) at the low-pressure region and vice-versa. There is a region of high pressure at the leading edge, stagnation point where the pressure is upto 1.26×10^3 Pa and region of low pressure on the upper surface of airfoil is -6.06×10^3 Pa (Fig.3)

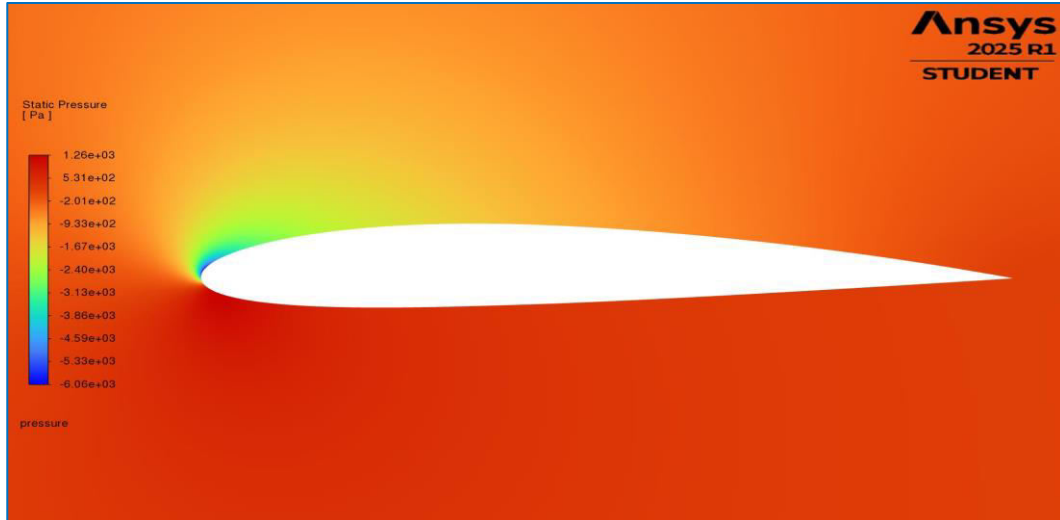


Figure 3: Static pressure contours over NACA 2412 airfoil at 6 degrees of AOA

2. Velocity magnitude over NACA 2412 airfoil:

Figures 4 and 5 demonstrate that at a 0-degree angle of attack (AOA), the velocity contours display symmetry. At a 6-degree AOA with a constant air flow of 45m/s, the stagnation point moves slightly toward the trailing edge along the bottom surface, producing a region of reduced velocity beneath the airfoil and an area of accelerated velocity above it. According to Bernoulli's principle, this creates lower pressure on the upper surface and elevated pressure on the lower surface. As a result, the lift coefficient rises, although the drag coefficient also increases, the rise in drag is minimal relative to the increase in lift force.

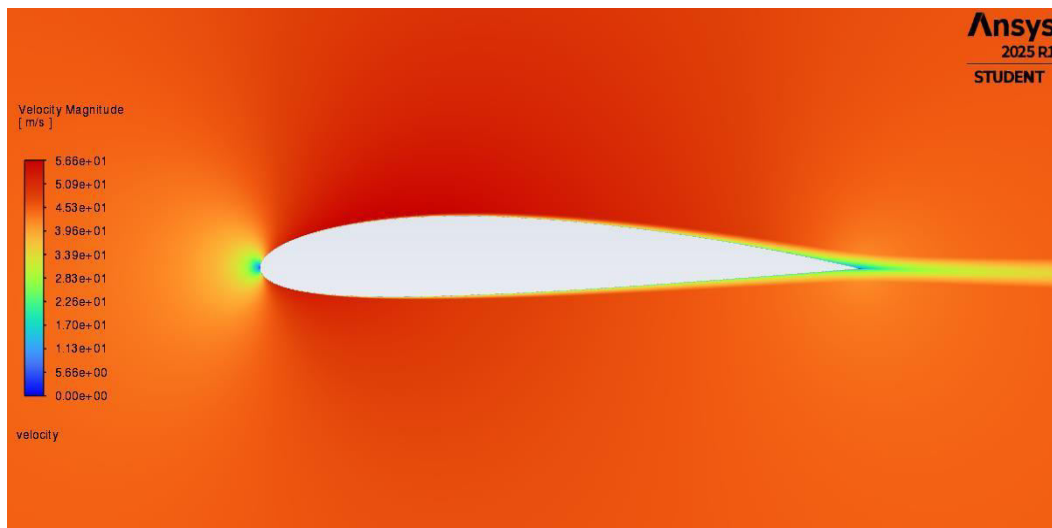


Figure 4: Velocity contour over NACA 2412 airfoil at 0 degree of AOA

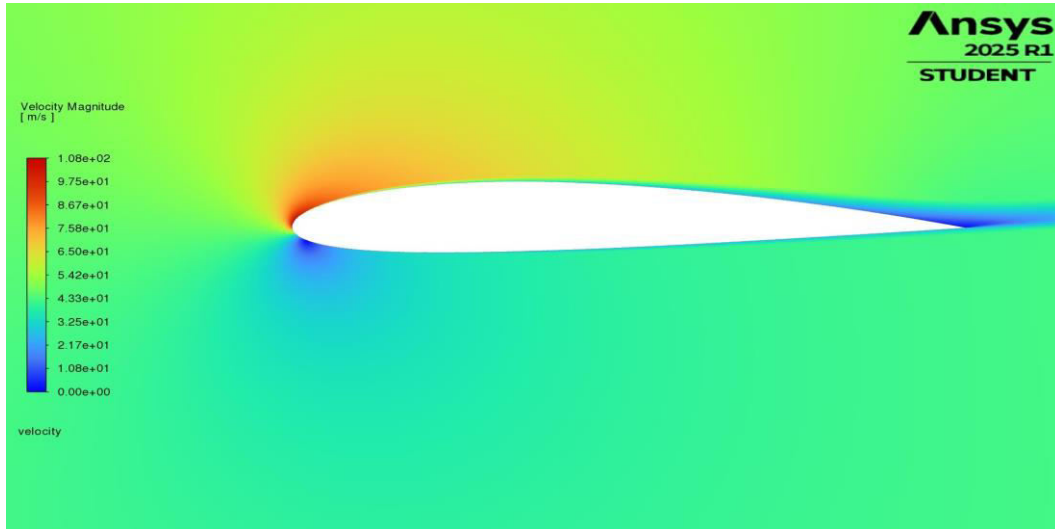


Figure 5: Velocity contour over NACA 2412 airfoil at 6 degrees of AOA

3. Validation of the CFD Model

To validate the precision of the CFD model, the lift and lift-to-drag ratio curves were compared with the experimental results reported by Abbott and Doenhoff [16], at a Reynolds number of 3.1×10^6 . Figure 7 presents a comparison between the experimental lift coefficients and those derived from CFD simulation. The lift coefficients show excellent alignment for angles of attack ranging from at 4° . Beyond an angle of attack of 4° , the results remain in good agreement, though the experimental lift coefficients slightly exceed the CFD values it is within margin of error. The error percentage for the CFD results against the experimental results is 1.814%

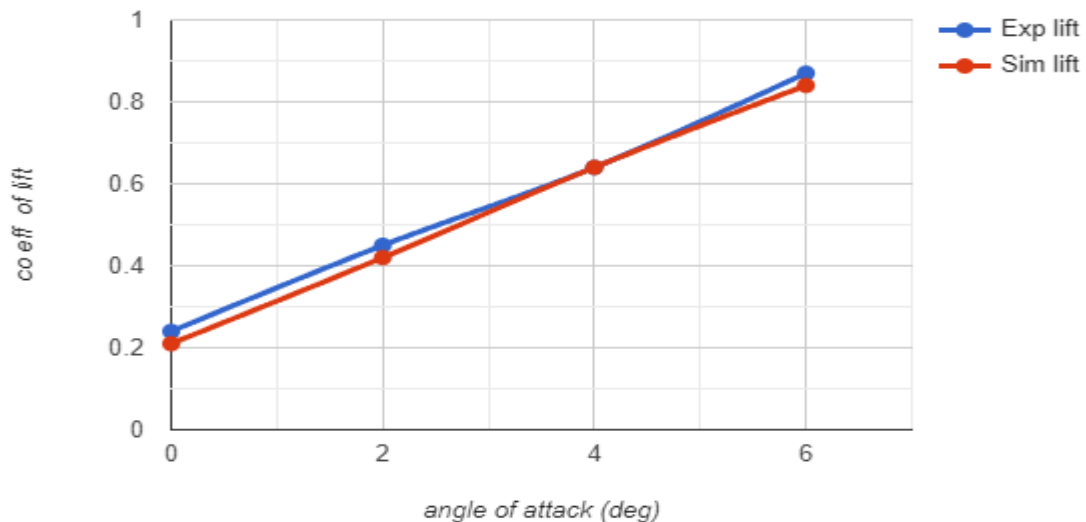


Fig.6 Comparison of lift coefficients obtained from CFD simulations with the available experimental data[9]

IV. DISCUSSION

In this study, the characteristics of NACA 2412 airfoils were investigated at different angle attacks. According to the results it is clear that with increasing AOAs, the lift coefficients were increasing. The highest lift coefficient was

obtained for an AOA of 14 degree with the value of 1.5512 at $Re = 3.1 \times 10^6$.

At 16-degree AOA, the NACA 2412 airfoil started to stall and did not produce any lift. Comparing the lift coefficients of the NACA airfoil, it is clear that the experimental data matches the CFD aerodynamic performances.

Based on the CFD analysis of the flow over NACA 0012 airfoil it is concluded that for a zero degree of AOA, there is no lift force generated and by increasing the AOA the lift force and lift coefficient tends to increase. The augment in AOA, the drag force and drag coefficient also increase but it is many fold smaller than the lift force. The 24% thickness of NACA 2124 offer structural advantages, reducing the need for internal reinforcements and potentially lowering manufacturing costs.

V. CONCLUSION

The salient conclusion of the present study are:

1. CFD is a very useful and reliable method that can be used to reduce cost for the manufacturing and testing of an airfoil.
2. Even at 0° angle of attack there is a considerable amount of lift generated which can be useful in various applications.
3. The velocity is constant throughout the experiment for the different angle of attack.
4. The numerical simulation results are concurrent with experimental results.
5. NACA 2124 airfoil is excellent for light and small aircraft because of its high lift at low speeds characteristics.

REFERENCES

- [1] Tirandaz, M.R. and Rezaeiha, A., 2021. Effect of airfoil shape on power performance of vertical axis wind turbines in dynamic stall: Symmetric Airfoils. *Renewable Energy*, 173, pp.422-441.
- [2] Cakmakcioglu, S.C., Bas, O., Mura, R. and Kaynak, U., 2020. A revised one-equation transitional model for external aerodynamics. In *AIAA aviation 2020 forum* (p. 2706).
- [3] Prajapati, G.M., Pathan, A. and Patel, M.B., 2014. A Review: Aerodynamic Analysis on Vertical Axis Wind Turbine Blade. *International Journal of Advance Engineering and Research Development*, 1(12).
- [4] Sreejith, B.K. and Sathyabhama, A., 2018. Numerical study on effect of boundary layer trips on aerodynamic performance of E216 airfoil. *Engineering science and technology, an international journal*, 21(1), pp.77-88.
- [5] Li, X., Zhang, L., Song, J., Bian, F. and Yang, K., 2020. Airfoil design for large horizontal axis wind turbines in low wind speed regions. *Renewable Energy*, 145, pp.2345-2357.
- [6] Kostić, I.A., Stefanović, Z.A. and Kostić, O.P., 2014. Aerodynamic analysis of a light aircraft at different design stages. *FME Transactions*, 42(2), pp.94-105.
- [7] Sabangban, N., Panagant, N., Bureerat, S., Wansasueb, K., Kuma, S., Yildiz, A.R. and Pholdee, N., 2023. Simultaneous aerodynamic and structural optimisation of a low-speed horizontal-axis wind turbine blade
- [8] Menter, F., Hüppe, A., Matyushenko, A. and Kolmogorov, D., 2021. An overview of hybrid RANS-LES models developed for industrial CFD. *Applied Sciences*, 11(6), p.2459.
- [9] Elsakka, M., 2020. The aerodynamics of fixed and variable pitch vertical Axis wind turbines (Doctoral dissertation, University of Sheffield).
- [10] Zohary, A.C., Asrar, W. and Aldheeb, M., 2021. Numerical investigation on the pressure drag of some low-speed airfoils for UAV application. *CFD Letters*, 13(2), pp.29-48.
- [11] Celik, Y., Ma, L., Ingham, D. and Pourkashanian, M., 2020. Aerodynamic investigation of the start-up process of H-type vertical axis wind turbines using CFD. *Journal of Wind Engineering and Industrial Aerodynamics*, 204, p.104252.
- [12] Manwell, J.F., McGowan, J.G. and Rogers, A.L., 2010. *Wind energy explained: theory, design and application*. John Wiley & Sons.
- [13] Einkemmer, L. and Joseph, I., 2021. A mass, momentum, and energy conservative dynamical low-rank scheme for the Vlasov equation. *Journal of Computational Physics*, 443, p.110495.
- [14] Prantl, L., Ummenhofer, B., Koltun, V. and Thuerey, N., 2022. Guaranteed conservation of momentum for learning particle-based fluid dynamics. *Advances in Neural Information Processing Systems*, 35, pp.6901- 6913.
- [15] Ansys Fluent 2024
- [16] Abbott, I. H. and von Doenhoff, A. E. (1959), *Theory of Wing Sections*, Dover Publications, New York.



INTERNATIONAL
STANDARD
SERIAL
NUMBER
INDIA



INTERNATIONAL JOURNAL OF INNOVATIVE RESEARCH

IN SCIENCE | ENGINEERING | TECHNOLOGY

 9940 572 462  6381 907 438  ijirset@gmail.com



www.ijirset.com

Scan to save the contact details